AGU ADVANCING EARTH AND SPACE SCIENCE

Geophysical Research Letters®

RESEARCH LETTER
10.1029/2022GL102123

Pacific Decadal Oscillation Influences Tropical Oxygen Minimum Zone Extent and Obscures Anthropogenic Changes

Mathieu A. Poupon[1,2], Laure Resplandy[1,3], Marina Lévy[4], and Laurent Bopp[5]

[1]Department of Geosciences, Princeton University, Princeton, NJ, USA, [2]Atmospheric and Oceanic Sciences Program, Princeton University, Princeton, NJ, USA, [3]High Meadows Environmental Institute, Princeton University, Princeton, NJ, USA, [4]LOCEAN-IPSL, CNRS, Sorbonne Université, Paris, France, [5]LMD/IPSL, ENS, Université PSL, École Polytechnique, Institut Polytechnique de Paris, Sorbonne Université, CNRS, Paris, France

Key Points:

- Pacific Decadal Oscillation (PDO) modulates tropical Pacific oxygen content and oxygen minimum zone volume on decadal time scales
- The PDO-induced variations are of the same order of magnitude as the anthropogenic deoxygenation signal
- Currently available data are too sparse to resolve and isolate the PDO-induced and anthropogenic signals

Supporting Information:

Supporting Information may be found in the online version of this article.

Correspondence to:

M. A. Poupon,
mpoupon@princeton.edu

Citation:

Poupon, M. A., Resplandy, L., Lévy, M., & Bopp, L. (2023). Pacific decadal oscillation influences tropical oxygen minimum zone extent and obscures anthropogenic changes. *Geophysical Research Letters*, *50*, e2022GL102123. https://doi.org/10.1029/2022GL102123

Received 16 NOV 2022
Accepted 20 MAR 2023

Abstract Observations suggest that the tropical Pacific Ocean has lost oxygen since the 1960s leading to the expansion of its oxygen minimum zone (OMZ). Attribution to anthropogenic forcing is, however, difficult because of limited data availability and the large natural variability introduced by the Pacific Decadal Oscillation (PDO). Here, we evaluate the PDO influence on oxygen dynamics and OMZ extent using observations and hindcast simulations from two global ocean circulation models (NEMO-PISCES, MOM6-COBALT). In both models, the tropical Pacific oxygen content decreases by about 30 Tmol.decade^{-1} and the OMZ volume expands by 1.3×10^5 km^3.decade^{-1} during PDO positive phases, while variations of similar magnitude but opposite sign are simulated during negative phases. Changes in equatorial advective oxygen supply, partially offset by biological demand, control the oxygen response to PDO. Observations which cover 39% of the tropical Pacific volume only partially capture spatio-temporal variability, hindering the separation of anthropogenic trend from natural variations.

Plain Language Summary Human activities cause oxygen loss in the ocean, which leads to the expansion of areas with very low oxygen concentrations located in the tropics called oxygen minimum zones (OMZ). Understanding the dynamics of OMZs is crucial because they produce greenhouse gasses and are unsuitable for the life of most large marine organisms. Quantifying the response of OMZs is however complicated by natural variability that superimposes on human-induced changes. In the Pacific Ocean, one of the strongest natural variability phenomena is the Pacific Decadal Oscillation. We used data and numerical models to assess the magnitude of oxygen changes caused by this natural phenomena in the tropical Pacific Ocean, and show that they are comparable to that of human-induced oxygen changes. We highlight that more oxygen data is needed to accurately separate natural variations from human-induced changes, and that a fraction of the oxygen loss attributed to human activities in prior work could in fact be due to natural variability.

1. Introduction

Since 1960, the ocean has lost 1%–2% of its global oxygen content (Helm et al., 2011; Ito et al., 2017; Schmidtko et al., 2017). In the tropical Pacific, in situ observations suggest that the deoxygenation rate is between −0.1 and −0.3 μmol.kg^{-1}.yr^{-1} (30°N–30°S in upper 1,000 m, Helm et al., 2011; Ito et al., 2017; Long et al., 2016; Schmidtko et al., 2017; Stramma et al., 2012), and Earth system models project that it will continue during the 21st century at a rate ranging from −0.05 to −0.1 μmol.kg^{-1}.yr^{-1} if emissions are not curtailed (i.e., under high emission scenarios, Bopp et al., 2013, 2017; Kwiatkowski et al., 2020; Levin, 2018; Long et al., 2016; Oschlies et al., 2017). The tropical Pacific hosts the world's largest oxygen minimum zone (OMZ), which has likely expanded in response to this substantial deoxygenation (Helm et al., 2011; Ito et al., 2017; Keeling et al., 2010; Schmidtko et al., 2017; Stramma et al., 2008). Deoxygenation is particularly critical near OMZs since the expansion of their volume threatens ecosystems by reducing niches of many macro-organisms such as tunas and marlins (Breitburg et al., 2018; Stramma et al., 2010, 2012; Vaquer-Sunyer & Duarte, 2008), and affects the production of nitrous oxide, a potent greenhouse gas (Babbin et al., 2015; Yang et al., 2020). While global deoxygenation is unambiguously attributed to anthropogenic warming, it is still unclear to which extent changes in the tropical Pacific OMZ volume are obscured by natural variability (Busecke et al., 2019; Deutsch et al., 2014; Ito & Deutsch, 2010; Ito et al., 2019; Long et al., 2016; Oschlies et al., 2017), partly because oxygen data are relatively sparse and sampling has been heterogeneous in this region over the last decades (Ito et al., 2017).

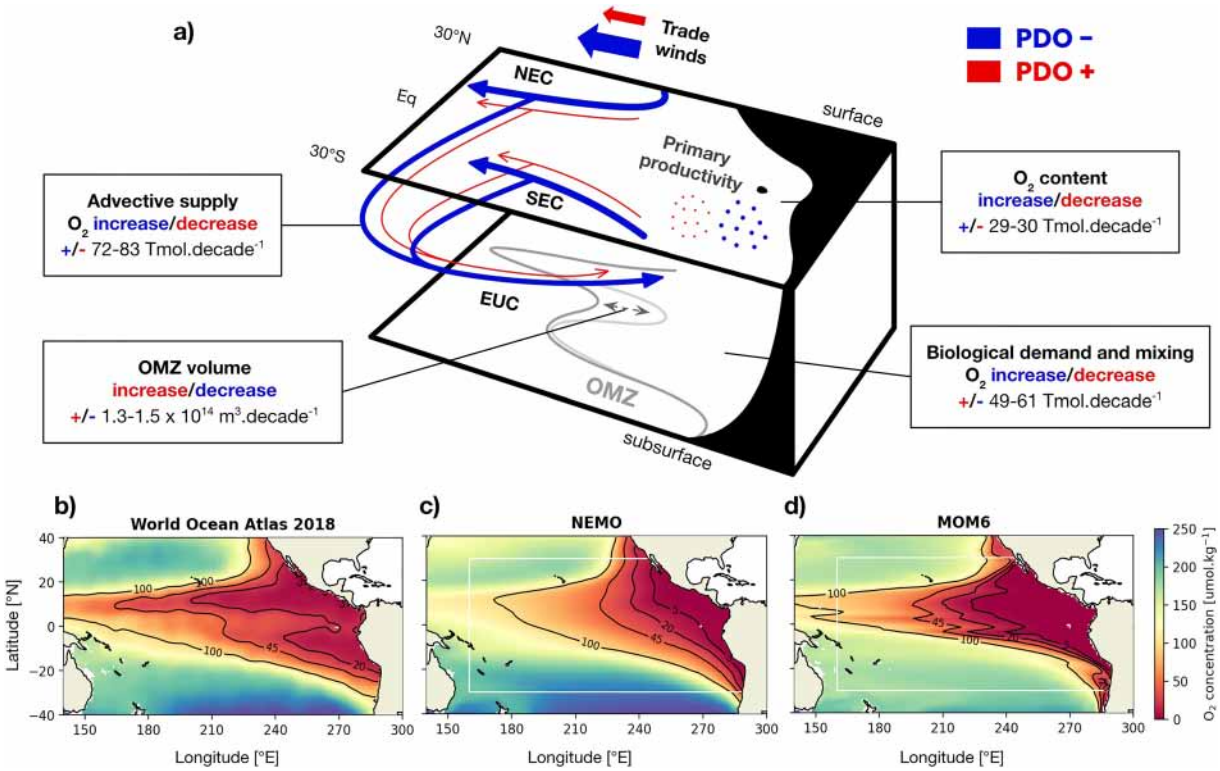

Figure 1. Processes controlling the tropical Pacific Ocean oxygen and OMZ variability during PDO positive (red) and negative (blue) phases. Main ocean circulation pathways: north equatorial current (NEC), south equatorial current (SEC), equatorial undercurrent (EUC, adapted from Duteil et al. (2018) to reflect the results of current study). Oxygen concentration at 400 m in (b) the World Ocean Atlas 2018, (c) the MOM6 (1959–2020) and (d) NEMO (1958–2019) model simulations. Black lines correspond to oxygen iso-concentrations: 5, 20, 45, 100 μmol.kg^{-1}. The white box in panels (d and e) delimits the study area.

The Pacific Decadal Oscillation (PDO, Mantua et al., 1997) is a major source of oxygen natural variability in the tropical Pacific on decadal time-scales (Duteil et al., 2018; Ito et al., 2019). Oxygen concentrations at the subsurface, where the OMZ is located, are controlled by the balance between biological demand and physical supply by the subtropical cells and the equatorial undercurrent (Figure 1a, e.g., Brandt et al., 2015; Busecke et al., 2019). The PDO modulates both the physical and the biological processes that control oxygen supply and consumption. During positive phases, trade winds slacken, causing a slowdown of subtropical cells (Hong et al., 2014) and the associated oxygen supply to the subsurface tropical Pacific (Duteil et al., 2014, 2018; Ito et al., 2019), while the vertical movement of isopycnals deepens the eastern tropical oxycline (Ito et al., 2019) as well as the thermocline leading to reduced respiration and oxygen demand (Deutsch et al., 2011, 2014). Negative phases are associated with the opposed response, including a more vigorous oxygen supply by subtropical cells and increased oxygen demand. Duteil and co-authors showed that circulation changes exceeded biological changes and that the OMZ volume was larger in an idealized ocean model experiment of perpetual positive PDO than in a companion experiment of perpetual negative PDO (Duteil et al., 2018).While these idealized experiments have clearly shown that the PDO has potential to induce significant OMZ volume changes, the magnitude of variations caused by a realistic PDO, which switches phase on decadal time scales and how it affects our ability to estimate and attribute the anthropogenic trend, has not been estimated yet.

Here we use two biophysical hindcast simulations reproducing the PDO's historical oscillations and an oxygen data product (Ito et al., 2017) both covering the past ~60 years to study and quantify the PDO impact on oxygen dynamics in the tropical Pacific. First, we show that PDO-induced changes in oxygen content and OMZ volume are of the same order of magnitude as those previously attributed to anthropogenic climate change. We find that the poor spatial and temporal observation coverage in this region does not allow to resolve these natural decadal variations, nor to attribute long-term trends. Finally we identify the mechanisms responsible for these variations.

2. Methods

2.1. Two Ocean Biophysical Models

We used hindcast simulations from two ocean biophysical models: (a) the Modular Ocean Model version 6 (MOM6, Adcroft et al., 2019) coupled with the Carbon, Ocean Biogeochemistry and Lower Trophics biogeochemical module version 2 (COBALT, Stock et al., 2020) developed by the Geophysical Fluid Dynamics Laboratory (GFDL), and (b) the Nucleus for European Modeling of the Ocean version 3.6 (NEMO, Madec et al., 2017) coupled with the Pelagic Interactions Scheme for Carbon and Ecosystem Studies biogeochemical module version 2 (Aumont et al., 2015) developed by the Institute Pierre-Simon Laplace (IPSL). COBALT and PISCES are intermediate complexity biogeochemical modules including 33 and 24 state variables respectively (e.g., 3 and 2 phytoplanktons, 3 and 2 zooplanktons, and nutrients such as nitrogen, phosphorus, iron and silica). The nominal horizontal resolution is 0.5° for MOM6 (i.e., 0.5° in longitude and 0.25° in latitude at the equator increasing to 0.45° at 30°N–30°S) and 1° for NEMO (1° in longitude and 0.3° in latitude at the equator increasing to 1° at 30°N–30°S). Both simulations are forced by the Japanese atmospheric reanalysis products (JRA55-do version 1.3 and 1.4, Tsujino et al., 2018 for MOM6 and NEMO, respectively). MOM6 was run for 1959–2020 after a 81 years spin up (see details in Liao et al. (2020)) and NEMO was run for 1958–2019 after a 122 years spin up (see details in Friedlingstein et al. (2020)). Results are presented for the upper tropical Pacific (0–1,000 m, 30°S–30°N, 160°E-eastern coast, see white box in Figures 1c and 1d).

We define the OMZ as the volume of water where the oxygen concentration is less than 45 $\mu mol.kg^{-1}$. However, as we discussed in the result section, the conclusions of this study are similar for all thresholds between 20 and 100 $\mu mol.kg^{-1}$ (Figure S3 in Supporting Information S1). For the analysis, we removed the 62-year deoxygenation and OMZ expansion trends (associated with processes with periods greater than the PDO, such as model drift or anthropogenic forcing) from the oxygen concentration (-45 $Tmol.decade^{-1}$ or -0.5 $\mu mol.kg^{-1}.decade^{-1}$ in NEMO, -10 $Tmol.decade^{-1}$ or -0.1 $\mu mol.kg^{-1}.decade^{-1}$ in MOM6, which represents respectively a change of -0.48% and $-0.11\%.decade^{-1}$ relative to the mean state) and OMZ volume ($+5.6 \times 10^{14}$ $m^3.decade^{-1}$ in NEMO, $+9.7 \times 10^{14}$ $m^3.decade^{-1}$ in MOM6 which represents respectively a change of $+2.82\%$ and $+3.74\%.decade^{-1}$ relative to the mean state) time-series in both simulations.

The MOM6 and NEMO simulations represent the main features of the Pacific OMZ (Figures 1b–1d). Including the horizontal footprint of the volume delimited by the 45 $\mu mol.kg^{-1}$ oxygen isoconcentration extending from 20°S to 39°N and from 220°E to the American continent at the equator. Simulated oxygen fields in the upper tropical Pacific (0–1,000 m, 30°S–30°N, 160°E-eastern coast, see white box in Figures 1c and 1d) have an average RMSE of 18.3 $\mu mol.kg^{-1}$ in MOM6 and 20.3 $\mu mol.kg^{-1}$ in NEMO compared to the World Ocean Atlas 2018 (WOA18) oxygen concentration climatology. Notable biases are a factor of two overestimation of the suboxic volume (<20 $\mu mol.kg^{-1}$) in MOM6 (17.6×10^{15} m^3, vs. 8.6×10^{15} m^3 in WOA18 and 9.0×10^{15} m^3 in NEMO), and a poor representation of the Equatorial undercurrent (EUC, Busecke et al., 2019), and off-equatorial alternating jets, either in the upper or lower thermocline (Duteil et al., 2021) which prevent the separation of the equatorial OMZ into a northern and southern lobe in NEMO (Figures 1b–1d).

2.2. Observational Data

We use the oxygen data product created by Ito et al. (2017) covering the upper 1,000 m of the ocean over the period 1958–2015 to estimate the amplitude of decadal variations in observations. We use data from four tropical ocean atmosphere (TAO) moorings collected monthly at the equator (0°N) almost continuously from 1988 to the present at longitudes: 165°E, 190°E, 220°E, 250°E, and distributed by NOAA (https://www.pmel.noaa.gov/gtmba/) to evaluate the simulated meridional velocity in the two models. We also used oxygen data from the WOA18 (Garcia et al., 2019) available online to evaluate the simulations.

2.3. Earth System Model Ensemble

We used the oxygen fields produced by 14 latest generation Earth system models from the Coupled Model Intercomparison Project Phase 6 (CMIP6, Eyring et al., 2016). Namely we use the following models: ACCESS-ESM1-5, CNRM-ESM2-1, CanESM5-CanOE, CanESM5, GFDL-CM4, GFDL-ESM4, IPSL-CM6A-LR,MIROC-ES2L, MPI-ESM1-2-HR, MPI-ESM1-2-LR, MRI-ESM2-0, NorESM2-LM, NorESM2-MM, UKESM1-0-LL. The

linear trend in dissolved oxygen contained in the study area (0–1,000 m, 30°S–30°N, 160°E-eastern coast) between 1958 and 2014 was evaluated for the first member of each model. We compared these trends to the oxygen content decadal variations induced by the PDO in the same region in the two models forced by past atmospheric conditions (NEMO, MOM6) and in the observation-based product.

2.4. Attribution of Oxygen Variability

We decompose oxygen variations (ΔO_2) into a thermal component tied to changes in solubility ($\Delta O_{2,sat}$) calculated using a python implementation of the TEOS-10 Gibbs SeaWater Oceanographic Toolbox (McDougall & Barker, 2011) and a non-thermal component tied to changes in circulation and biological activity (apparent oxygen utilization variation, ΔAOU). ΔAOU can be further decomposed into a large-scale transport term related to the renewal of oxygen by advective transport (AdvTransport), computed offline using annual mean simulated field of apparent oxygen utilization gradient and velocity fields, and a residual term capturing the effects of biological activity and mixing (BioMix):

$$\begin{aligned}\Delta O_2 &= \Delta O_{2,sat} - \Delta AOU \\ &= \Delta O_{2,sat} - \int_t^{t+\Delta t} \left(\frac{\partial AOU}{\partial t}\right) dt \\ &= \Delta O_{2,sat} \underbrace{+ \int_t^{t+\Delta t} \left(\vec{v} \cdot \vec{\nabla} AOU\right) dt}_{\text{AdvTransport}} \underbrace{- \int_t^{t+\Delta t} \left(D\nabla^2 AOU + J_{Bio}\right) dt}_{\text{BioMix}}\end{aligned}$$

Where D is the diffusion coefficient and J_{Bio} the oxgyen biological production/consumption.

2.5. Identifying PDO Signal

We used the monthly PDO index data distributed by NOAA (https://psl.noaa.gov/pdo/) to track PDO phase changes. We retained decadal variations associated with the PDO using a temporal butterworth low-pass filter with a cutoff period of 16 years that removes high frequency variations associated with shorter variability modes such as ENSO (Figure S1 in Supporting Information S1). During the simulation period, the PDO index is characterized by two negative phases (1958–1976 and 1998–2015) and a positive phase (1977–1997, Figure S1 in Supporting Information S1). Oxygen fields (oxygen concentration, OMZ volume and oxygen budget terms) were filtered using the same approach to remove frequencies higher than 16 years and retain the signal associated with the PDO.

3. Results

3.1. PDO Control Over Tropical Pacific Oxygen Content and OMZ Volume

The oxygen content in the upper tropical Pacific (0–1,000 m, 30°S–30°N, 160°E-eastern coast) increases during PDO negative phases and decreases during positive phases in both the NEMO and MOM6 simulations (solid lines in Figure 2a). We find that the oxygen content change is negatively correlated with the PDO index in both models (Figure S2a in Supporting Information S1). On average over the three PDO phases, the net change in oxygen amounted to ±29 Tmol.decade^{-1} (±0.32 µmol.kg^{-1}.decade^{-1}) in NEMO and ±30 Tmol.decade^{-1} (±0.33 µmol.kg^{-1}.decade^{-1}) in MOM6 (Figure 2a), which correspond to changes of ±0.30% and ±0.33%.decade^{-1} in total oxygen content. The two models suggest, however, that the magnitude of the oxygen response to PDO varied in time, with higher oxygenation rates found during the first negative phase (+38 and +35 Tmol.decade^{-1} in NEMO and MOM6 between 1958 and 1976) compared to the most recent negative phase (+22 and +29 Tmol.decade^{-1} between 1998 and 2015), and to the deoxygenation rates found during the positive phase (−29 and −31 Tmol.decade^{-1} between 1977 and 1997, Figure 2a).

We compare the simulated oxygen decadal variations to the observation-based data product from Ito et al. (2017). Observations are sparse and only cover 39% of the tropical Pacific volume, we therefore use oxygen concentrations instead of total oxygen content in this comparison (Figure 2c). The data set shows a decadal oxygen variability of ±0.9 µmol.kg^{-1}.decade^{-1} in phase with the PDO, consisting of an average gain of +1.5 µmol.kg^{-1}.decade^{-1} during the first negative phase and a loss of −1.1 µmol.kg^{-1}.decade^{-1} during the positive phase, but surprisingly stable oxygen concentrations during the last negative phase (−0.01 µmol.kg^{-1}.decade^{-1}, Figure 2c). This later

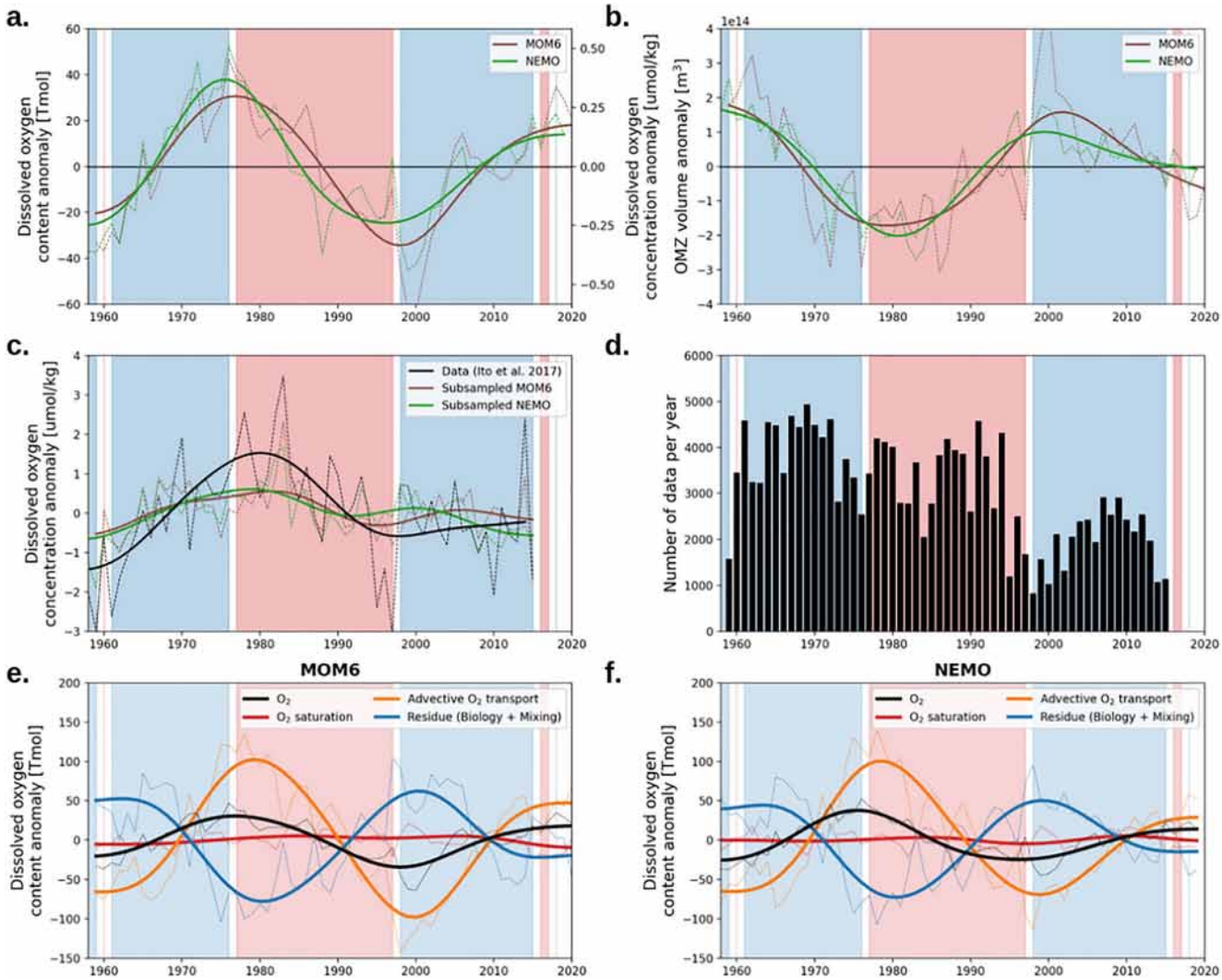

Figure 2. Observed and modeled oxygen variability in the upper tropical Pacific (0–1,000 m, 30°S–30°N, 160°E-Eastern coast). Time series of (a) oxygen content (in Tmol) and concentration (in umol.kg^{-1}) anomalies and (b) OMZ volume anomaly in the MOM6 (brown) and NEMO (green) simulations. Time series of (c) oxygen concentration anomaly time series in Ito et al. (2017) data (black), and subsampled at the data location in the MOM6 (brown) and NEMO (green) simulations and (d) amount of data for each year in the Ito et al. data set. Changes in oxygen content (black), and contributions from changes in solubility (O2sat, red), advective transport (orange) and residual variations tied to biological activity and mixing (blue) in the (e) MOM6 and (f) NEMO simulations. In panels (a–c) and (e, f), the thin dotted lines are the annual signals and the thick solid lines are the filtered decadal signals (obtained by applying a 16-years low pass filter on the annual signals). Blue and red shadings indicate periods of negative and positive PDO phases.

period is, however, the least sampled, with on average 2,034 observations per year versus 3,525 per year for the earlier period (Figure 2d). These observed oxygen changes are almost four times larger than those simulated in the models (±0.25 μmol.kg^{-1}.decade^{-1} in MOM6, and ±0.23 μmol.kg^{-1}.decade^{-1} in NEMO). We assess the effect of heterogeneous sampling in space and time by subsampling the simulated oxygen fields at the location of available observations (solid colored lines in Figure 2c). Once subsampled, the simulated oxygen changes amplitude increases by a factor two during the first two PDO phases and is almost zero during the last and least sampled period, improving the match with the data (Figure 2c, $r^2 = 0.59$ vs. 0.18 in NEMO, r^2: 0.28 vs. 0.19 in MOM6, Figure S2 in Supporting Information S1). The fact that the subsampled models is well correlated with the data, but poorly with the full model results ($r^2 = 0.04$ in NEMO and 0.1 in MOM6, Figure S2 in Supporting Information S1) suggests that the data coverage is not sufficient to capture the spatial and temporal variations associated with the PDO.

Decadal changes in oxygenation influence the simulated volume of the tropical Pacific OMZ which contracts during negative PDO phases and expands during positive phases (Figure 2b). In both models the rate of change

in OMZ volume (defined here as $[O_2] < 45$ μmol.kg^{-1}) is similar, amounting to $\pm 1.3 \times 10^{14}$ m^3.decade^{-1} (corresponding to ±0.37%.decade^{-1}) in NEMO and $\pm 1.5 \times 10^{14}$ m^3.decade^{-1} (±0.27%.decade^{-1}) in MOM6 (Figure 2b). Note that the tight link between PDO phases and OMZ volume rate of change shown here for the OMZ defined with an oxygen threshold of 45 μmol.kg^{-1} is robust and significant across all oxygen thresholds between 20 and 120 μmol.kg^{-1} (Figure S3 in Supporting Information S1). Spatially, we find that these changes in oxygen content and OMZ volume simulated in response to the PDO in the tropical Pacific Ocean (30°S–30°N) are controlled by changes in the equatorial region (10°S–10°N, see Figures S4 and S5 in Supporting Information S1). In contrast, the northern (10°N–30°N) and southern (30°S–10°S) tropics experience smaller amplitude modulations associated with oxygen spatial redistributions which are only weakly correlated with the PDO (Figures S4–S6 in Supporting Information S1).

3.2. Key Role of Equatorial Oxygen Supply on Decadal Time-Scales

In both simulations, decadal oxygen variations in the upper tropical Pacific are controlled by variations in advective transport (Figures 2e and 2f). Advective oxygen transport is stronger during negative phases and weaker during positive phases, resulting in an increase in oxygen content during negative phases and a decrease during positive phases, with change rates of ±72 Tmol.decade^{-1} in NEMO and ±83 Tmol.decade^{-1} in MOM6. Transport modulations also control surface nutrient supply and productivity, as well as subsurface organic carbon export and biological demand, and oxygen gradient changes alter mixing. Thus, changes in oxygen supply due to advective transport are offset up to 70% by changes in biological activity and mixing (±49 and ±61 Tmol.decade^{-1} in NEMO and MOM6 respectively, Figures 2e and 2f). Taken together, these non-thermal changes (advection, biology and mixing) represent variations ±27 Tmol.decade^{-1} in NEMO and ±29 Tmol.decade^{-1} that largely explain the net oxygen changes associated with PDO phases (±29 Tmol.decade^{-1} and $r^2 = 0.96$ in NEMO, ±30 Tmol.decade^{-1} and $r^2 = 0.96$ in MOM6). In contrast, solubility-induced changes in oxygen content are of a lower order of magnitude and show no significant correlation with PDO phases (Figures 2e and 2f, $r^2 = 0.1$ in NEMO and 0.04 in MOM6). Consistent with the key contribution of the equatorial band to oxygen and OMZ changes, we find that the 10°S–10°N band controls the changes induced by non-thermal processes in the 30°S–30°N band (Figure S7 in Supporting Information S1).

Over the simulation period, more than 70% of the oxygen supply by advective transport to the equatorial Pacific (0–1,000 m, 10°S–10°N, 160°E-Eastern coast) occurs between 2°S and 2°N (72% in NEMO and 79% in MOM6), and is sustained by the EUC that transports subsurface oxygenated waters eastward (Figures 3a and 3b). The EUC supplies +387 Gmol.yr^{-1} in NEMO and +642 Gmol.yr^{-1} in MOM6 to the upper equatorial Pacific. On the other hand, the jets on either side of the equatorial undercurrent transport low oxygen waters westward (Figures 3a and 3b, −58 Gmol.yr^{-1} in NEMO and −79 Gmol.yr^{-1} in MOM6). These jets are better represented in MOM6 because of the higher horizontal resolution and lower numerical dissipation near the equator, which explains their higher impact on the oxygen budget. In both models, the oxygen transport by the equatorial undercurrent and the jets is modulated by 5%–8% due to the changes in circulation associated with PDO phases. During PDO positive phase, the oxygen supply by the equatorial undercurrent weakens (−26 Gmol.yr^{-1}, −6.6% relative to the mean state in NEMO and −45 Gmol.yr^{-1}, −7.5% in MOM6), while during negative phases, the transport increases (+17 Gmol.yr^{-1}, +4.5% in NEMO and +34 Gmol.yr^{-1}, +5.6% in MOM6, Figures 3c–3f).

Oxygen observations are too sparse to estimate decadal variations in oxygen transport. However, since the zonal subsurface oxygen gradient is a persistent feature of the equatorial Pacific, mass transport variability, which we can infer from the zonal velocity measured at the TAO moorings, is a good proxy for oxygen transport variability. On average over the TAO moorings measurement period (1988-present), the simulated EUC amplitude and westward shallowing following the thermocline are realistic compared to observations (Figures 3g–3j, RMSE on climatological zonal velocities of 0.17 m.s^{-1} for NEMO and 0.12 m.s^{-1} for MOM6). For three of the four moorings (moorings at 190°E, 220°E, and 250°E), the zonal mass transport in the top 300 m is larger during the negative phases than the positive phase, as reproduced in the 2 simulations (Figures 3h–3j). These results are also consistent with previous work (Kuntz & Schrag, 2021). In contrast, we see that the transport at the most western mooring (165°E) which does not measure the EUC core responds differently, with higher transport during the positive phase than negative phases (Figure 3g). We note that the models reproduce the sign of change expected from the observations but underestimate the amplitude of the variations up to a factor two (amplitudes of 4.4% ± 4.3% in observations vs. 1.3% ± 1.7% in NEMO and 1.9% ± 2.5% in MOM6). This suggests that the mass

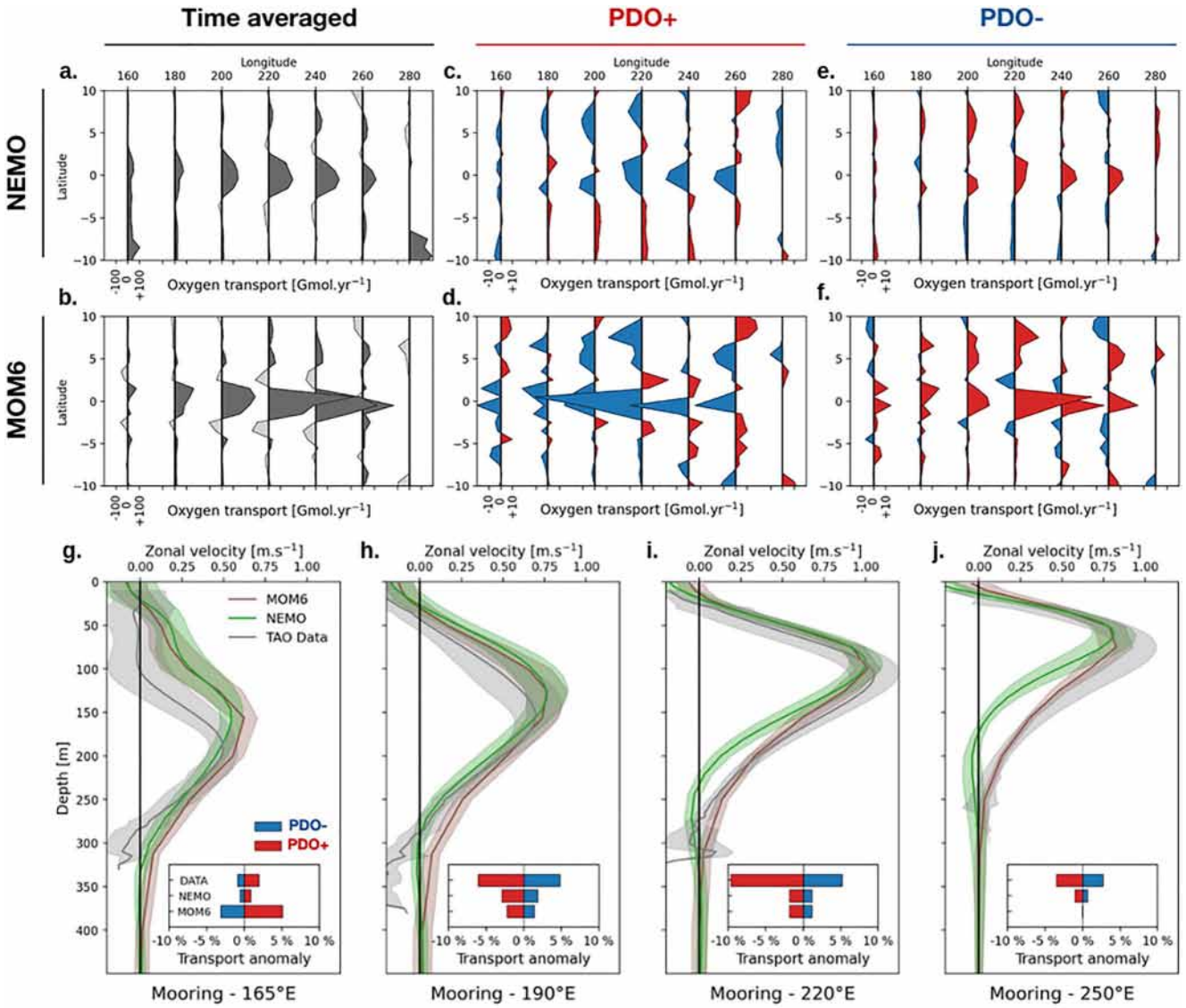

Figure 3. Zonal advective oxygen transport integrated over the top 1,000 m as a function of latitude in the NEMO (top row) and MOM6 (bottom row) models: (a), (b) mean transport for the 1958–2020 period and anomalies relative to the mean state during (c), (d) positive and (e), (f) negative PDO phases. Positive transports are eastward. In panels (c–f), red areas indicate an increase in oxygen supply by ocean currents while blue areas indicate a decrease. Model-data comparison for four equatorial Tropical Ocean Atmosphere (TAO) moorings located at (g) 165°E, (h) 190°E, (i) 220°E and (j) 250°E. Mean zonal velocity profiles (solid lines) and interannual variability (±1 standard deviation indicated as shading) in the MOM6 simulation (brown), NEMO simulation (green) and TAO data set (gray). For each panel, the insert is the transport anomaly integrated between 40 and 250 m, relative to the mean state during positive (red) and negative (blue) PDO phases over the period covered by the TAO observations.

transport decadal variability, and by extension the influence of PDO on the advective oxygen transport, might be underestimated by the models in the equatorial band.

4. Conclusion and Discussion

Using two ocean general circulation biophysical simulations, we show that, during negative PDO phases, the upper tropical Pacific oxygen content increases by about 30 Tmol.decade^{-1} (±0.33 µmol.kg^{-1}.decade^{-1}). The intensification of ocean currents in the upper tropical Pacific, in particular the equatorial undercurrent, increases the oxygen supply to the OMZ ($O_2 < 45$ µmol.kg^{-1}) leading to its contraction at a rate of 1.3×10^5 km^3.decade^{-1}. In contrast, during positive PDO phases, the supply by the equatorial undercurrent weakens, the oxygen content decreases and the OMZ expands by a similar amount (Figure 1b). Up to 70% of the oxygen variations tied

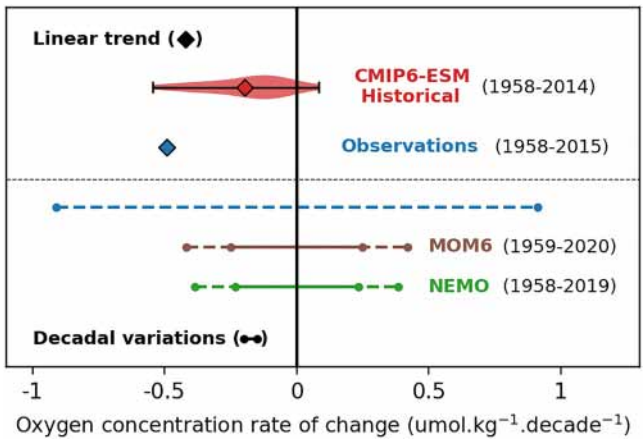

Figure 4. Mean oxygen concentration change rate (squares) in the upper tropical Pacific (0–1,000 m, 30°S–30°N, 160°E-Eastern Coast), in the observation-based product of Ito et al. (2017) (blue, 1958–2015) and in the CMIP6-ESM historical simulations (red, 1958–2014). The colored area is the trend distributions for the different models. Decadal variations in mean oxygen concentration (lines) in the product of Ito et al. (blue), in the MOM6 (brown, 1959–2020) and NEMO (green, 1958–2019) simulations. The solid lines are the averaged decadal variation rates over the full basin, while the dashed lines is for a basin subsampled at locations where observations are available.

to advective transport are offset by changes in biology and mixing. These results are consistent with velocity measurements from the TAO moorings and oxygen observations from Ito et al. (2017) available between 1958 and 2020 in the tropical Pacific. The key role of advective transport, biological demand and mixing is consistent with the work of Duteil et al. (2018), which suggested that oxygen changes in the equatorial suboxic zone (<20 μmol.kg^{-1}) are controlled by advective processes. Here we identify a net change in the oxygen transport into the tropical Pacific subsurface in response to PDO phases. This is different from the east/west redistribution of oxygen in the upper layer (associated with the vertical movement of isopycnals during PDO phases) identified in Ito et al. (2019), which modulates the depth of the oxycline but has little influence on the volume of the tropical OMZ. Furthermore, we find that the tropical changes in integrated oxygen content and OMZ volume associated with the PDO are controlled by the 10°S–10°N band, while weaker oxygen redistribution is simulated in the northern and southern tropics.

PDO-induced changes in oxygen estimated in this study using ocean models and observations are of the order of 0.25–0.90 μmol.kg^{-1}.decade^{-1} (Figure 4). The observation-based estimate is, however, about three times higher than that simulated by the two models (±0.90 vs. ±0.25 μmol.kg^{-1}.decade^{-1}). Two factors contribute to this model-observation mismatch in the oxygen response. First, we find that data undersampling artificially amplifies oxygen decadal variability, as suggested by the larger variations obtained when subsampling the models similarly to observations compared to using the full model solution (from ±0.25 vs. ±0.40 μmol.kg^{-1}.decade^{-1}, compare solid/dashed brown and green lines in Figure 4). Second, the two ocean models likely underestimate natural oxygen decadal variability. Indeed, the simulated variability in advective mass transport, which is a good indicator of oxygen transport, is only one third of that measured by the TAO buoys. However, we note that the model bias in advective transport would likely lead to a smaller oxygen bias (only half when comparing dashed lines in Figure 4), because of the strong compensation between advective oxygen supply and biological demand in this region. The equatorial surface productivity and subsurface biological demand are tied to the ocean dynamics intensity supplying nutrients.

Changes in oxygen associated with the PDO are likely to obscure the anthropogenic deoxygenation trend and bias its estimates over the historical period (1958–2014). The oxygen concentration changes induced by the PDO estimated here (about ±0.25 μmol.kg^{-1}.decade^{-1} in models and ±0.9 μmol.kg^{-1}.decade^{-1} in observations, Figure 4) are of the same order of magnitude as the deoxygenation trends estimated over a similar period using an ensemble of the latest generation of Earth system model (CMIP6) historical experiments (−0.2 ± 0.2 μmol.kg^{-1}.decade^{-1}, 1958–2014, Figure 4), as well as the observation-based data set of Ito and co-authors (−0.5 μmol.kg^{-1}.decade^{-1}, 1958–2015, Figure 4). Long-term human-driven oxygen loss and PDO-related oscillations in oxygen concentrations are therefore superimposed, and isolating them in the historical observations remains a challenge. Oxygen observations are sparse and require interpolations over large space-time domains which we show here introduce biases when inferring long-term trends in this region. In addition, most oxygen observations in the region were taken in the past 60 years which only covers 3 PDO cycles and limits the attribution of the trend to climate change. This is in line with Earth system models suggesting that the human-driven deoxygenation signal may only emerge in about 30–40 years in the tropical Pacific Ocean (Long et al., 2016; Schlunegger et al., 2019).

Data Availability Statement

Model data used to perform this analysis are available on zenodo (Currently on Zenodo Sandbox: https://sandbox.zenodo.org/record/1129979).

Acknowledgments
The study has been supported by the High Meadows Environmental Institute Grand Challenge and L.R. NSF CAREER award number 2042672.

References

Adcroft, A., Anderson, W., Balaji, V., Blanton, C., Bushuk, M., Dufour, C. O., et al. (2019). The GFDL global ocean and sea ice model OM4.0: Model description and simulation features. *Journal of Advances in Modeling Earth Systems*, *11*(10), 3167–3211. https://doi.org/10.1029/2019MS001726

Aumont, O., Ethé, C., Tagliabue, A., Bopp, L., & Gehlen, M. (2015). PISCES-v2: An ocean biogeochemical model for carbon and ecosystem studies. *Geoscientific Model Development*, *8*(8), 2465–2513. https://doi.org/10.5194/gmd-8-2465-2015

Babbin, A. R., Bianchi, D., Jayakumar, A., & Ward, B. B. (2015). Rapid nitrous oxide cycling in the suboxic ocean. *Science*, *348*(6239), 1127–1129. https://doi.org/10.1126/science.aaa8380

Bopp, L., Resplandy, L., Orr, J. C., Doney, S. C., Dunne, J. P., Gehlen, M., et al. (2013). Multiple stressors of ocean ecosystems in the 21st century: Projections with CMIP5 models. *Biogeosciences*, *10*(10), 6225–6245. https://doi.org/10.5194/bg-10-6225-2013

Bopp, L., Resplandy, L., Untersee, A., Le Mezo, P., & Kageyama, M. (2017). Ocean (de)oxygenation from the Last Glacial Maximum to the twenty-first century: Insights from Earth system models. *Philosophical Transactions of the Royal Society A: Mathematical, Physical & Engineering Sciences*, *375*(2102), 20160323. https://doi.org/10.1098/rsta.2016.0323

Brandt, P., Bange, H. W., Banyte, D., Dengler, M., Didwischus, S.-H., Fischer, T., et al. (2015). On the role of circulation and mixing in the ventilation of oxygen minimum zones with a focus on the eastern tropical North Atlantic. *Biogeosciences*, *12*(2), 489–512. https://doi.org/10.5194/bg-12-489-2015

Breitburg, D., Levin, L. A., Oschlies, A., Grégoire, M., Chavez, F. P., Conley, D. J., et al. (2018). Declining oxygen in the global ocean and coastal waters. *Science*, *359*(6371), eaam7240. https://doi.org/10.1126/science.aam7240

Busecke, J. J. M., Resplandy, L., & Dunne, J. P. (2019). The equatorial undercurrent and the oxygen minimum zone in the Pacific. *Geophysical Research Letters*, *46*(12), 6716–6725. https://doi.org/10.1029/2019GL082692

Deutsch, C., Berelson, W., Thunell, R., Weber, T., Tems, C., McManus, J., et al. (2014). Centennial changes in North Pacific anoxia linked to tropical trade winds. *Science*, *345*(6197), 665–668. https://doi.org/10.1126/science.1252332

Deutsch, C., Brix, H., Ito, T., Frenzel, H., & Thompson, L. (2011). Climate-forced variability of ocean hypoxia. *Science*, *333*(6040), 336–339. https://doi.org/10.1126/science.1202422

Duteil, O., Böning, C. W., & Oschlies, A. (2014). Variability in subtropical-tropical cells drives oxygen levels in the tropical Pacific Ocean. *Geophysical Research Letters*, *41*(24), 8926–8934. https://doi.org/10.1002/2014GL061774

Duteil, O., Frenger, I., & Getzlaff, J. (2021). The riddle of eastern tropical Pacific Ocean oxygen levels: the role of the supply by intermediate-depth waters. *Ocean Science*, *17*(5), 1489–1507. https://doi.org/10.5194/os-17-1489-2021

Duteil, O., Oschlies, A., & Böning, C. W. (2018). Pacific decadal oscillation and recent oxygen decline in the eastern tropical Pacific Ocean. *Biogeosciences*, *15*(23), 7111–7126. https://doi.org/10.5194/bg-15-7111-2018

Eyring, V., Bony, S., Meehl, G. A., Senior, C. A., Stevens, B., Stouffer, R. J., & Taylor, K. E. (2016). Overview of the Coupled Model Intercomparison Project Phase 6 (CMIP6) experimental design and organization. *Geoscientific Model Development*, *9*(5), 1937–1958. https://doi.org/10.5194/gmd-9-1937-2016

Friedlingstein, P., O'Sullivan, M., Jones, M. W., Andrew, R. M., Hauck, J., Olsen, A., et al. (2020). Global carbon budget 2020. *Earth System Science Data*, *12*(4), 3269–3340. https://doi.org/10.5194/essd-12-3269-2020

Garcia, H., Boyer, T., Baranova, O., Locarnini, R., Mishonov, A., Grodsky, A. E., et al. (2019). *World ocean atlas 2018: Product documentation*. In A. Mishonov (Ed.), Technical Editor, 1, 1–20.

Helm, K. P., Bindoff, N. L., & Church, J. A. (2011). Observed decreases in oxygen content of the global ocean. *Geophysical Research Letters*, *38*(23), L23602. https://doi.org/10.1029/2011GL049513

Hong, L., Zhang, L., Chen, Z., & Wu, L. (2014). Linkage between the Pacific decadal oscillation and the low frequency variability of the Pacific subtropical cell. *Journal of Geophysical Research: Oceans*, *119*(6), 3464–3477. https://doi.org/10.1002/2013JC009650

Ito, T., & Deutsch, C. (2010). A conceptual model for the temporal spectrum of oceanic oxygen variability. *Geophysical Research Letters*, *37*(3), L03601. https://doi.org/10.1029/2009GL041595

Ito, T., Long, M. C., Deutsch, C., Minobe, S., & Sun, D. (2019). Mechanisms of low-frequency oxygen variability in the North Pacific. *Global Biogeochemical Cycles*, *33*(2), 110–124. https://doi.org/10.1029/2018GB005987

Ito, T., Minobe, S., Long, M. C., & Deutsch, C. (2017). Upper ocean O_2 trends: 1958–2015. *Geophysical Research Letters*, *44*(9), 4214–4223. https://doi.org/10.1002/2017GL073613

Keeling, R. F., Körtzinger, A., & Gruber, N. (2010). Ocean deoxygenation in a warming world. *Annual Review of Marine Science*, *2*(1), 199–229. https://doi.org/10.1146/annurev.marine.010908.163855

Kuntz, L. B., & Schrag, D. P. (2021). Subtropical modulation of the equatorial undercurrent: A mechanism of Pacific variability. *Climate Dynamics*, *56*(5), 1937–1949. https://doi.org/10.1007/s00382-020-05568-w

Kwiatkowski, L., Torres, O., Bopp, L., Aumont, O., Chamberlain, M., Christian, J. R., et al. (2020). Twenty-first century ocean warming, acidification, deoxygenation, and upper-ocean nutrient and primary production decline from CMIP6 model projections. *Biogeosciences*, *17*(13), 3439–3470. https://doi.org/10.5194/bg-17-3439-2020

Levin, L. A. (2018). Manifestation, drivers, and emergence of open ocean deoxygenation. *Annual Review of Marine Science*, *10*(1), 229–260. https://doi.org/10.1146/annurev-marine-121916-063359

Liao, E., Resplandy, L., Liu, J., & Bowman, K. W. (2020). Amplification of the Ocean carbon sink during El Niños: Role of poleward Ekman transport and influence on atmospheric CO_2. *Global Biogeochemical Cycles*, *34*(9), e2020GB006574. https://doi.org/10.1029/2020GB006574

Long, M. C., Deutsch, C., & Ito, T. (2016). Finding forced trends in oceanic oxygen. *Global Biogeochemical Cycles*, *30*(2), 381–397. https://doi.org/10.1002/2015GB005310

Madec, G., Bourdallé-Badie, R., Bouttier, P.-A., Bricaud, C., Bruciaferri, D., Calvert, D., et al. (2017). NEMO ocean engine. (Report). https://doi.org/10.5281/zenodo.3248739

Mantua, N. J., Hare, S. R., Zhang, Y., Wallace, J. M., & Francis, R. C. (1997). A Pacific interdecadal climate oscillation with impacts on Salmon production. *Bulletin of the American Meteorological Society*, *78*(6), 1069–1080. https://doi.org/10.1175/1520-0477(1997)078⟨1069:APICOW⟩2.0.CO;2

McDougall, T., & Barker, P. (2011). Getting started with TEOS-10 and the Gibbs Seawater (GSW) oceanographic toolbox. *Scor/Iapso WG*, *127*, 1–28.

Oschlies, A., Duteil, O., Getzlaff, J., Koeve, W., Landolfi, A., & Schmidtko, S. (2017). Patterns of deoxygenation: Sensitivity to natural and anthropogenic drivers. *Philosophical Transactions of the Royal Society A: Mathematical, Physical & Engineering Sciences*, *375*(2102), 20160325. https://doi.org/10.1098/rsta.2016.0325

Schlunegger, S., Rodgers, K. B., Sarmiento, J. L., Frölicher, T. L., Dunne, J. P., Ishii, M., & Slater, R. (2019). Emergence of anthropogenic signals in the ocean carbon cycle. *Nature Climate Change*, *9*(9), 719–725. https://doi.org/10.1038/s41558-019-0553-2

Schmidtko, S., Stramma, L., & Visbeck, M. (2017). Decline in global oceanic oxygen content during the past five decades. *Nature*, *542*(7641), 335–339. https://doi.org/10.1038/nature21399

Stock, C. A., Dunne, J. P., Fan, S., Ginoux, P., John, J., Krasting, J. P., et al. (2020). Ocean biogeochemistry in GFDL's Earth system model 4.1 and its response to increasing atmospheric CO_2. *Journal of Advances in Modeling Earth Systems*, *12*(10), e2019MS002043. https://doi.org/10.1029/2019MS002043

Stramma, L., Johnson, G. C., Sprintall, J., & Mohrholz, V. (2008). Expanding oxygen-minimum zones in the tropical oceans. *Science*, *320*(5876), 655–658. https://doi.org/10.1126/science.1153847

Stramma, L., Prince, E. D., Schmidtko, S., Luo, J., Hoolihan, J. P., Visbeck, M., et al. (2012). Expansion of oxygen minimum zones may reduce available habitat for tropical pelagic fishes. *Nature Climate Change*, *2*(1), 33–37. https://doi.org/10.1038/nclimate1304

Stramma, L., Schmidtko, S., Levin, L. A., & Johnson, G. C. (2010). Ocean oxygen minima expansions and their biological impacts. *Deep Sea Research Part I: Oceanographic Research Papers*, *57*(4), 587–595. https://doi.org/10.1016/j.dsr.2010.01.005

Tsujino, H., Urakawa, S., Nakano, H., Small, R. J., Kim, W. M., Yeager, S. G., et al. (2018). JRA-55 based surface dataset for driving ocean–sea-ice models (JRA55-do). *Ocean Modelling*, *130*, 79–139. https://doi.org/10.1016/j.ocemod.2018.07.002

Vaquer-Sunyer, R., & Duarte, C. M. (2008). Thresholds of hypoxia for marine biodiversity. *Proceedings of the National Academy of Sciences of the United States of America*, *105*(40), 15452–15457. https://doi.org/10.1073/pnas.0803833105

Yang, S., Chang, B. X., Warner, M. J., Weber, T. S., Bourbonnais, A. M., Santoro, A. E., et al. (2020). Global reconstruction reduces the uncertainty of oceanic nitrous oxide emissions and reveals a vigorous seasonal cycle. *Proceedings of the National Academy of Sciences of the United States of America*, *117*(22), 11954–11960. https://doi.org/10.1073/pnas.1921914117